Chemical Engineering Journal 457 (2023) 141209

Contents lists available at ScienceDirect

Chemical Engineering Journal

journal homepage: www.elsevier.com/locate/cej

High-performance aggregation-induced emission active poly(ether sulfone)s as polymeric electret for energy-saving genuine photonic transistor memory

Chun-Yao Ke, Mu-Huai Chen, Guey-Sheng Liou *

Institute of Polymer Science and Engineering, National Taiwan University, No. 1, Sec. 4, Roosevelt Road, Taipei 10617, Taiwan

ARTICLE INFO

Keywords:
AIE polymers
Triphenylamine
Poly(ether sulfone)
Polymer electrets
Photonic Transistor Memory

ABSTRACT

Next-generation photo-driven memory devices and artificial neuromorphic networks have shown great promise in adopting organic photo-recordable devices because of their tremendous merits, highly tailorable structures, facile processing, and low power consumption. There are generally-two operation approaches, light-assistant and genuine methods, that can be divided into categories based on whether to apply electrical biasing (V_{GS} or V_{DS}) during the photo-programming process. The genuine type manifests glamorous characteristics in optical communication and neural computation due to the exclusion of additional electric consumption. Nevertheless, there is a lack of investigation into the relationship between the genuine photo-programming process and the design strategy of polymeric electrets. This work is the first to employ triphenylamine (TPA)-based aggregation-induced emission (AIE)-active poly(ether sulfone)s as the electret layer of a photonic transistor memory device to elaborate photo-induced programming. Every chemical building block, AIE-active TPA, ether, and sulfone moieties, has been soundly elucidated and plays an indispensable role in possessing high-performance homo-polymer-based photonic memory, including enhancement of photo-induced recording, outstanding retention (14 days), and reducing the working voltage ($V_{GS} = 0$ V and $V_{DS} = -5$ V). This study presents an eye-catching design strategy for creating polymer-based photonic memory that also satisfies energy-saving criteria in practice.

1. Introduction

Nowadays, with an ever-increasing amount of information that needs to be calculated, accessed, and stored, the revolution of the optoelectronic device is urgently desired. To boost the data storage abilities of memories in modern electronics, scaling down is the mainstream for achieving high-density memory chips that face their bottleneck due to technical complexity [1]. Compared to typical electrical-driven memories, photo-driven memories that signal-readout are orthogonal to photo-modulating operations endow ultrafast transmission and low power consumption to ensure high output variance between different current levels. As a result, photonic memories inhere attractive merits for next-generation nonvolatile memories.

To obtain the photo-memory behavior, embedding charge storage components, such as metallic and semiconducting nanomaterials, or inserting blending type electret between the gate and semiconducting layer are the most common methods [2]. Among nanomaterials, inorganic quantum dots, polymer dots, and perovskite nanocrystals (PVSK NCs) have exhibited good photo-gating behavior due to the high photoluminescence quantum yields for triggering the photoexcitation excitons in the semiconducting layer followed by the separation of electron-hole pairs then. Chen et al. brought out the first hybrid composite composed of PS/perovskite and inspired a series following exploration and modification [3]. However, facing the dilemma of dispersion issues and specific morphology requirements. Thus, there is still a distance to practical large-area production for the blending systems.

In comparison, homogeneous polymeric electrets provide a facile method for fabricating organic field-effect transistor (OFET) memory devices [4–8]. Besides offering decent heat resistance and mechanical tolerance, polymer electrets are favorable even for severe process conditions. Recent advances in light-stimulated synaptic devices that employ polymeric gate dielectric materials have demonstrated excellent photo-induced programmability by reacting to transient optoelectronic stimuli [9–14]. To perform optical-writing processes, the polymer electret photonic devices should apply electric stress (gate voltage or

* Corresponding author.
E-mail address: gsliou@ntu.edu.tw (G.-S. Liou).

https://doi.org/10.1016/j.cej.2022.141209
Received 21 October 2022; Received in revised form 15 December 2022; Accepted 26 December 2022

drain voltage) during irradiation. Therefore, the phenomenon should refer to light-assisted electrical programming or optoelectronic stimulation. Although extensive studies on optoelectronic stimulative operation in photoresponsive polymeric electret OFET memory have been reported, there is a lack of investigation into the relationship between genuine photo-programming or optical stimulative operation and polymer electret design strategy, which would be a more energy-efficient operation strategy for next-generation optical communication systems due to the exclusion of additional electric energy consumption.

In our recent work, we designed and employed triphenylamine (TPA)-based conjugated polymers with photoresponsive pendent groups as the charge to unveil the enigma of the photo-induced storage layer of genuine photo-programmable OFET memory [15]. The mechanism investigated of photo-boosted recording behavior depicts the recombination of the formed interlayer excitons through appropriate energy-level alignment at the interface in-between active semiconductor and polymer electrets. Unfortunately, the high electric stress is still demanded on the flash-type device with PTPA-CN electret to eliminate the electron trapped by the photo-programing procedure, which would restrict the practicality of the application.

Herein, high-performance poly(ether sulfones) (PESs) derived from diphenolic monomers and 4,4′-difluorodiphenyl sulfone were adopted as electret layers of photonic transistor-type memory devices for the very first time, as illustrated in Fig. 1. Classic aggregation-induced emission (AIE)-gens, α-cyanostilbene (CNBr) and tetraphenylethylene (TPE), are attached to the TPA unit as the photo-active building block. Consequently, the PESs could achieve moderate photoluminescence (PL) quantum efficiency and appropriate energy level. Under genuine photo-programming, the TPE-PES and CNBr-PES memory devices demonstrate prominent memory windows of 10 V and 50 V, respectively, indicating the transfer curve would dramatically change toward the positive direction following light exposure without providing vertical and parallel electric stress. The isolation system produced by ether linkage offers reliable and durable information storage. Both PESs-based photonic devices could maintain the memory behavior for the last 100,000 s without significant dissipation. They can expect to preserve the switching ratio above 10^3 even over 10^9 s (approximately 32 years) through extrapolation calculations. Surprisingly, sulfone linkage could offer a favorable growth environment for pentacene to gain a large domain size with fewer crystal boundaries despite the relatively low hydrophobicity. As a result of the lower contact resistance between electrodes and semiconducting materials due to the large grain of pentacene, the operating voltage could reduce to 5 V [16]. Especially, TPE-PES with an extended conjugation length displaying a higher hole affinity can quickly neutralize electrons trapped in OFET device.

Significantly, compared to the recent emerging light-stimulated synaptic devices or organic photonic memory summarized in Table 1, our study not only realizes the simple photo-programming method without applying voltage but also observes the reduced erasing voltage, which is lower than that listed in the literature [9–14]. Namely, this work has achieved outstanding energy-saving performance in the recent development of organic photonic memory, implying that the well-designed polymer structures with exceptional AIE performance have received less attention in applying organic photonic memory [17–18]. To our knowledge, this is the first time incorporating a series PESs in photonic memory devices to effectively improve the high voltage issue that the polymeric electret faces by adopting a facile and low-cost polymerization method, making PES one of the potential candidates in the future photonic memory device operation methods to realize programming and erasing are highlighted in blue and brown colors.

2. Experimental section

2.1. Synthesis and characterization of monomer

The synthetic routes of the designed polymers and the corresponding FTIR spectra are depicted in Fig. 2. 4,4′-Dimethoxytriphenylamine (TPA-OMe), 1-[4-(bis(4-methoxyphenyl)amino)phenyl]1,2,2-triphenylethene (TPE-OMe), and 2-(4-bromophenyl)-3-[4-(bis(4-methoxyphenyl)amino)phenyl]acrylonitrile (CNBr-OMe) were prepared according to the previous reports [19–20]. Afterwards, 4,4′-dihydroxytriphenylamine (TPA-OH), 1-[4-(bis(4-hydroxyphenyl)amino)phenyl] 1,2,2-triphenylethene (TPE-OH), and 2-(4-bromophenyl)-3-[4-(bis(4-methoxyphenyl)amino)phenyl]acrylonitrile (CNBr-OH) were synthesized by demethylation reaction with high yields above 93% [21–22]. The diphenolic monomers are confirmed by NMR, FT-IR, and melting

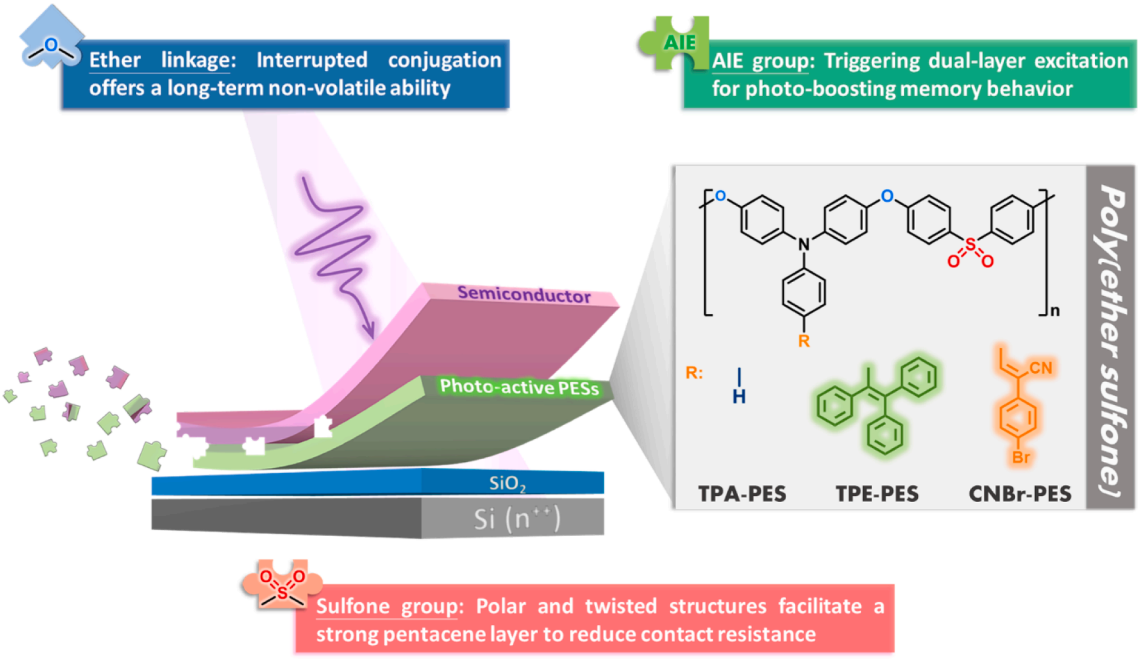

Fig. 1. Schematic diagram of the fabricated photonic memory devices and design strategies of each building block of photo-active PES electrets striving toward stable and low-consumption photo-programmable memory devices.

Table 1
Comparison of recently developed photonic memory devices or optical synaptic transistors, including floating-gate and polymer-type electrets. The Fig. 1. Schematic diagram of the fabricated photonic memory devices and design strategies of each building block of photo-active PES electrets striving toward stable and low-consumption photo-programmable memory devices.

SiO_2 thickness	Electret	Semiconductor	Programming Operation	Erasing operation	Classification	Ref.
100 nm	PVN blending with 30% PCBM	Pentacene	740 nm-light and V_{GS} of 20 V for 60 s	740 nm-light and V_{GS} of −20 V for 30 s	*Light-assisted electrical programming process/ Light-assisted electrical erasing process*	[9]
90 nm	PS/Al_2O_3/Ta_2O_5	Pentacene	635 nm-light and V_{GS} of 20 V for 300 s	–	*Light-assisted electrical programming process*	[10]
100 nm	PVN	Pentacene	254 nm-light and V_{GS} of 4 V for 1.5 s	254 nm-light and V_{GS} of −4 V for 2 s	*Light-assisted electrical programming process /Light-assisted electrical erasing process*	[11]
100 nm	Sol-PDI	BPEPDI	640 nm-light and V_{DS} of 40 V for 20 s	60 V above 5 s	*Light-assisted electrical programming process /Electrical erasing process*	[12]
100 nm	C10-DNTT	DNTT	405 nm-light and V_{DS} of −30 V for 20 s	60 V above 5 s	*Light-assisted electrical programming process /Electrical erasing process*	[12]
ITO	P4PMS	$F_{16}CuPc$	Illumination and V_{GS}/V_{DS} of 10 V/40 V for 10 s	Volatile	*Light-assisted electrical programming process*	[13]
300 nm	Layer-free	Pentacene	Illumination and V_{GS} of 100 V for 10 s	Illumination and V_{GS} of −100 V for 10 s	*Light-assisted electrical programming process/ Light-assisted electrical erasing process*	[14]
100 nm	TPE-PES	Pentacene	365 nm-light for 1 s **Without any V_{GS}/V_{DS}**	−10 V for 5 s	*Genuine photo-programming process/Electrical erasing process*	**This study**
100 nm	CNBr-PES	Pentacene	365 nm-light for 1 s **Without any V_{GS}/V_{DS}**	WORM-type	*Genuine photo-programming process*	**This study**

[9] *ACS Applied Materials & Interfaces* **2019**, 11, 40366–40371. [10] *Advanced Electronic Materials* **2020**, 6, 1901255. [11] *IEEE Electron Device Letters* **2022**, 43, 124–127. [12] *Advanced Materials* **2020**, 32, 2002638. [13] *ACS Applied Materials & Interfaces* **2010**, 2, 6, 1614–1620. [14] *Advanced Electronic Materials* **2022**, 8, 2101349.

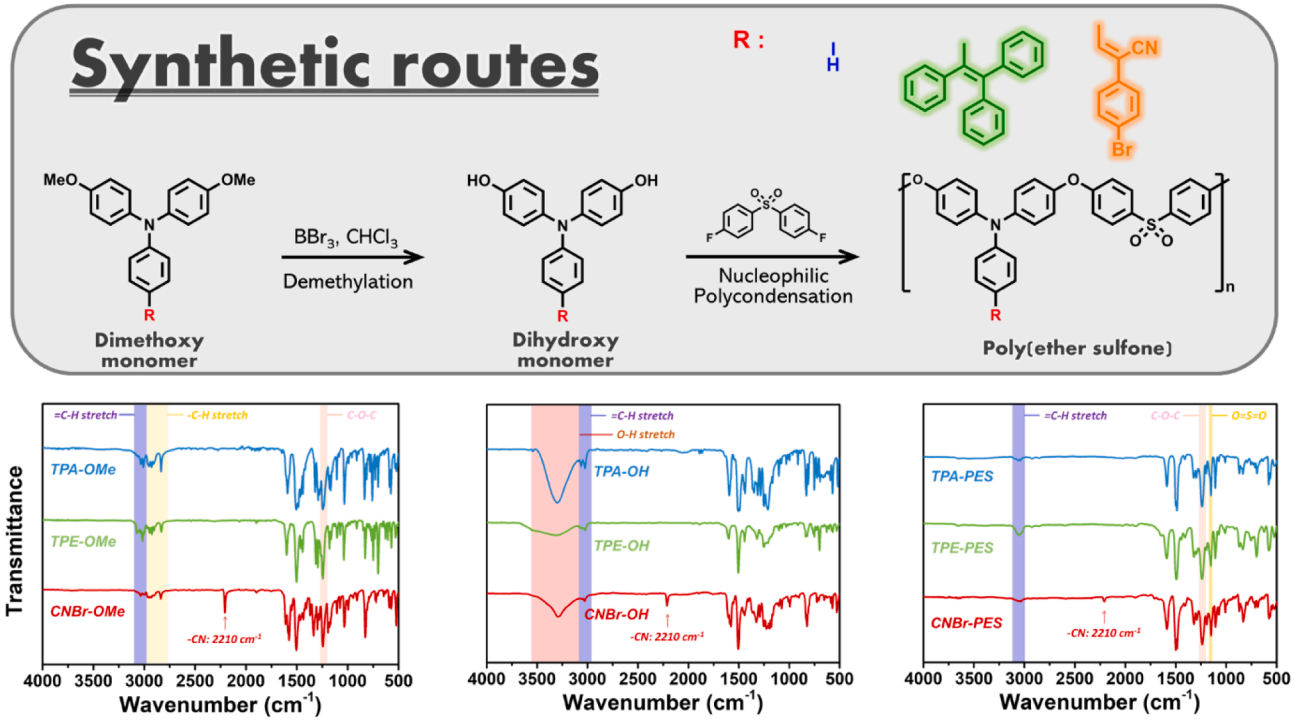

Fig. 2. Synthetic routes and corresponding FTIR spectra from dimethoxy intermediates and diphenol monomers to target PESs.

point measurements, as summarized in Fig. 2 and S1-S4. The peak from the hydroxyl group is around 9.3 ppm in ^{1}H NMR, O—H stretching around 3550–3200 cm^{-1} with the absence of aliphatic C—H stretching band around 3000–2800 cm^{-1}, and sharpness of melting point indicates the pure diphenolic monomers were ready for step-growth polymerization.

2.2. Synthesis and characterization of Poly(ether sulfone)s

TPA-based PESs, TPA-PES, TPE-PES, and CNBr-PES, were successfully synthesized *via* conventional aromatic nucleophilic substitution polycondensation, as shown in Fig. 2. After the polymerization, the crude product was washed thoroughly with methanol and water by a Soxhlet extractor, and the neat PESs with high yields could be prepared. The inherent viscosities and molecular weights of the obtained PESs are summarized in **Table S1**. It is worth noting that only an inexpensive and easily removed alkaline catalyst is necessary for this polycondensation. Consequently, this facile approach could significantly suppress the interference from residual metal catalysts in the electrical characteristic. ^{1}H NMR spectra of TPE-PES and CNBr-PES were also measured, as depicted in **Figures S5-S6**. FT-IR spectra of dimethoxy intermediates, diphenolic monomers, and the target PESs are illustrated in Fig. 2. The O—H stretching around 3550–3200 cm^{-1} disappears, while the C—O stretching of ether linkage appears near 1250 cm^{-1}, confirming the PESs

were successfully obtained.

3. Results and discussion

3.1. Thermal properties

Thermogravimetric analysis (TGA) and differential scanning calorimetry (DSC) was used to study the thermal stability properties of PESs (**Figures S7 and S8**), and the glass-transition temperatures (T_g), degradation temperature (T_d), and char yields are summarized in **Table S2**. In both nitrogen and air atmosphere, the produced PESs demonstrated remarkable thermal stability with insignificant weight loss up to 400 °C. Besides, TPA-based PESs possess a char yield above 47% at 800 °C. The T_g of PESs is from 188 °C to 220 °C. As a result, PESs could easily afford the high temperature in the following physical vapor deposition, one of the most common processes in optoelectronic devices.

3.2. Optical and electrochemical properties

The optical properties of PESs films investigated by ultraviolet–visible spectroscopy (UV–vis) and PL spectroscopy are depicted in Fig. 3 and summarize the corresponding data in **Table S3.** The characteristic absorption peak at 308 nm attributed to the TPA moiety π–π* transition and charge transfer peaks caused by the donor–acceptor interactions of TPE-PES and CNBr-PES appeared around 350 nm and 423 nm, respectively. Furthermore, the high transmittance in the visible region of TPE-PES suggests the potential for transparent and colorless electronics. In contrast, the appearance of CNBr-PES film is light yellowish, as shown in Fig. S9**a**. The AIE effect of PESs depicted in Fig. S9**b and S9c** could simulate the emission behavior from solution to solid states using the *N*-methyl-2-pyrrolidone (NMP) polymer solutions with different methanol fractions. The dilute NMP solutions of TPE-PES and CNBr-PES exhibit gradually enhanced PL intensity through mixing with an increasingly poor solvent of methanol to obtain the nano-scale aggregation. The AIE phenomenon of TPE could ascribe to the twisted propeller-shaped conformation hampering π-π stacking interaction and the restricted intramolecular rotations caused by physical constraint in the aggregate state, known as the restriction of intramolecular motions (RIM) mechanism. [23] Meanwhile, CNBr exhibits the AIE behavior because aggregation-induced planarization enhances oscillator strength; also, the bulky and polar cyano group precludes parallel face-to-face intermolecular interaction and provides intermolecular hydrogen bonding to rigidify molecules. [24] Thus, TPE-PES and CNBr-PES possess strong emissions in film state at 490 and 575 nm, respectively, as shown in the PL spectra.

The energy levels were investigated by the measurement of cyclic voltammetry (CV) using PES film-coated indium-tin-oxide (ITO) glass substrate as the working electrode in 0.1 M tetrabutylammonium perchlorate (TBAP)/anhydrous acetonitrile (CH_3CN) solution. **Figure S10** and Fig. 4 show the CV diagrams and accompanying energy levels, and **Table S4** summarizes the obtained results. With the extended conjugation length and acceptor on the side chain, TPE-PES/CNBr-PES possess lower energy levels of HOMO (-5.33 eV/-5.35 eV) and LUMO (-3.21 eV/-3.25 eV) and smaller bandgap compared to TPA-PES. The appropriate energy levels allow polymeric electret to perform a more effective energy transfer to pentacene and trigger the interlayer-exciton recombination between the interface. [15] The samples with single (AIE-active PESs) and double layer (pentacene deposited on AIE-active PESs) structures are analyzed via steady-state PL spectra, as shown in **Figure S19**. The occurrence of interlayer recombined excitons could be observed and exhibited an additional emission peak around 690–700 nm.

3.3. Surface morphology

The surface morphology plays an essential role in the OFET memory device because the charge transfer and trapping processes occur in the interfaces between semiconductor and electret layers. [25–26] To reveal the surface behaviors generated by PESs, BPA-PES, the most typical PES derived from bisphenol A, was also synthesized for the following discussion. According to the literature, pentacene is susceptible to surface roughness and hydrophobicity. [27–31] The favorable condition of pentacene growth on polymer electret, including the properties of low

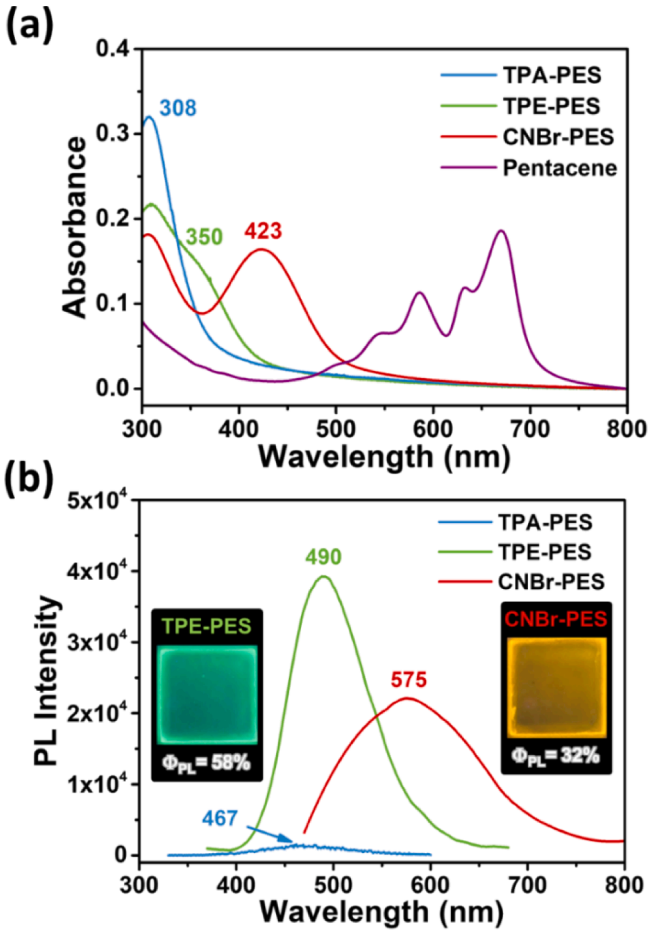

Fig. 3. (a) UV–vis absorption spectra and (b) PL emission spectra of spin-coated PESs films. (Thickness = 40 ± 2 nm).

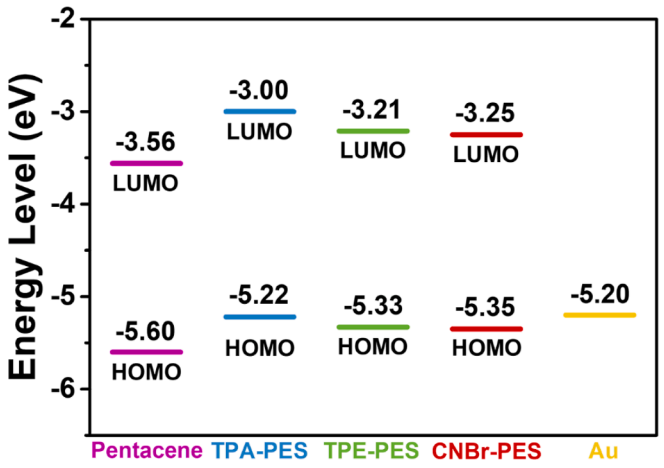

Fig. 4. The energy levels of pentacene and TPA-based PESs measured by cyclic voltammetry.

surface energy and the smooth electret surface, could improve the wettability of pentacene. The aqueous contact angles of BPA-PES, TPA-PES, TPA-PES, and CNBr-PES are 85°, 85°, 86°, and 89°, respectively, while the film roughness varies between 0.233 nm and 0.258 nm as depicted in **Figure S11**. BPA-PES, TPA-PES, and TPE-PES exhibit similar contact angles due to the hydrophobicity brought by alkyl chains and phenyl rings. In the case of CNBr-PES, introducing a bromine atom to the molecular structure increases hydrophobicity and gives it a higher contact angle [32–34]. In addition, the smooth and uniform surface also could minimize the defects or interfacial trapping between the semiconductor and electret, ensuring that the charge capture behaviors could ascribe to the chemical structure of polymer electrets. The typical terrace-like form of pentacene with average domain sizes from 1060 to 1570 nm could be produced as shown in the atomic force microscopy (AFM) topography of pentacene deposited on PESs.

Generally, as the hydrophobicity increases, larger grain sizes could be obtained to reduce crystal boundaries. However, pentacene with a larger grain size of around 1060 nm could be generated in the case of BPA-PES as electret, which exhibits poorer hydrophobicity than carbazoledioxazine-based polymer, Poly CD, reported previously by us, and the corresponding structures and data are summarized in **Table S5** for comparison [5]. Consequently, in addition to the effect caused by roughness and hydrophobicity, the larger grain size should be attributed to the difference between the structures of sulfone and carbazole-derivative. As Ji *et al.* reported in a previous study [35], the twisted conformation and highly polar functional groups on a molecular level are two crucial factors offering a repulsive interaction between the polymer and the π-electron clouds of the pentacene skeleton that leads to an ordered vertical orientation of pentacene and further expands into more prominent domains. To soundly corroborate the effect of these two units, the X-ray diffraction (XRD) measurement was designated to investigate the relationship between polymer structures and morphology characteristics. As illustrated in **Figure S20**, Pentacene thin films with different thicknesses (5, 20, and 50 nm) on BPA-PES exhibit (00 l) diffractions. In particular, the (0 0 1) diffraction pattern peak ($2\theta = 5.46°$) at the beginning step (5 nm) of the growth process yields a d_{001} spacing of 1.62 nm. This representative peak at $2\theta = 5.46°$ did not appear from pentacene films on Poly CD; instead, a relatively weak diffraction peak at $2\theta = 5.70°$ (d-spacing: 1.51 nm) was observed for 5 nm film, indicating a reasonably low crystallinity with a larger tilted angle of the pentacene molecules on the Poly CD surface. In other words, BPA-PES contains sulfone moiety providing higher polarity and more contorted conformation for facilitating a more beneficial growth environment of pentacene instead of the coplanar and more hydrophobic carbazole-derivative in Poly CD.

Consequently, contact resistance (R_C), the parameter determined by the interface between the materials of electrodes and semiconducting materials, could be reduced according to more significant grain boundaries of pentacene with fewer trapping sites and vice versa [16]. Reliable measurement and calculation for getting contact resistance (R_C) is the transfer line method (TLM), which is a direct application of equation (1) [36]. Plotting the data of $R_{total}W$ against channel length (L) with good linearity, RcW can be derived from the extrapolation, as presented in Fig. 5. The results indicate that the Poly CD with a smaller pentacene grain size possesses more significant contact resistance than BPA-PES with a larger pentacene grain size.

$$R_{total} = R_{ch} + R_C = \frac{L}{WC_i(V_{GS} - V_T)\mu_{ch}} + R_C \quad (1)$$

where V_{DS}, I_D, R_{total} are the drain voltage and corresponding current and total resistance; all of them is channel length dependence parameter. C_i, $V_{GS,}$ and W are the capacitance per unit area of the SiO_2 layer, gate bias, and channel width, respectively. Therein, an electrode of gold was then deposited onto the pentacene. The grain size of pentacene is the primary factor affecting R_C in this investigation. PESs could reduce the contact resistance between the semiconductor and electrode and give prominent surface properties.

3.4. Performance of pentacene-based photonic memory with PESs electrets

The OFET memory devices fabricated based on typical bottom-gate (BG) and top-contact (TC) configurations and PESs as electrets were adopted to study the photonic transistor memory characteristics, as illustrated in Fig. 1. All measurements were performed in the glove box with a blackout curtain (a genuinely dark and inert environment) to eliminate the interference of indoor light. The primary electrical hysteresis and output curves of PESs-based OFET memory devices are illustrated in Fig. 6 and **Figure S12**. The saturation regime field-effect mobility of pentacene-based memory devices was evaluated as depicted in **Figure S13** with estimated values of 0.03 $cm^2\ V^{-1}\ s^{-1}$. Meeting our expectations, all the memory devices fabricated by TPA-based PESs electrets could achieve the saturated region by only $V_{DS} = -5$ V.

Moreover, the read-out currents reveal that the higher current induced under the same gate bias as the acceptor units introduced in the side chain strengthens the dipole capability and accumulates more charges in the channel. Among the TPA-based PESs, CNBr-PES demonstrates the largest hysteresis window through dual-sweeping and elucidates that the extended conjugation length results in enhanced hole-

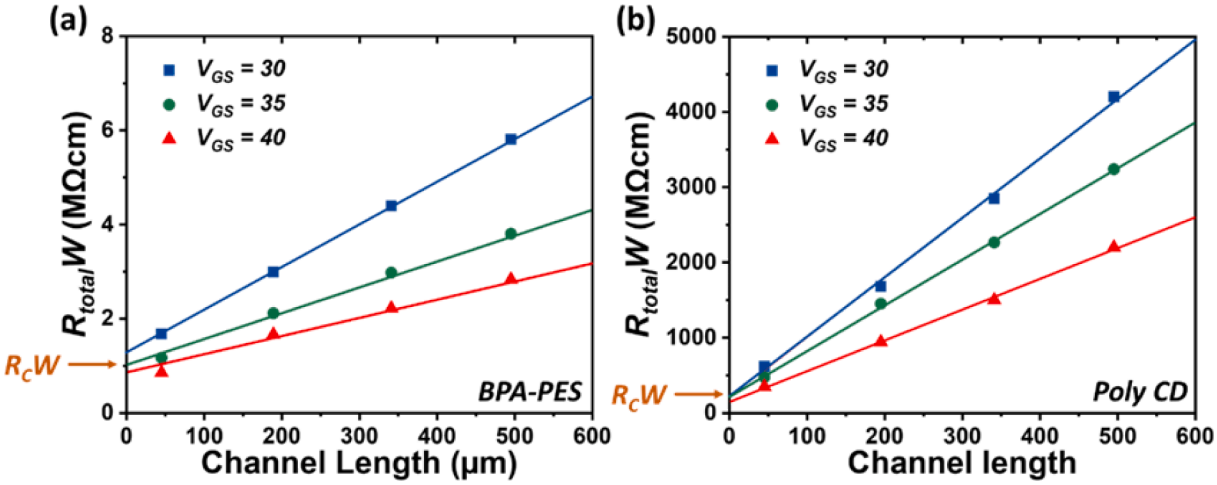

Fig. 5. Transistor total resistance vs channel length (TLM plots) for (a) BPA-PES and (b) Poly CD transistor memory devices. (Where Rc, BPA-PES is 0.001 MΩ, and Poly CD is 0.188 MΩ).

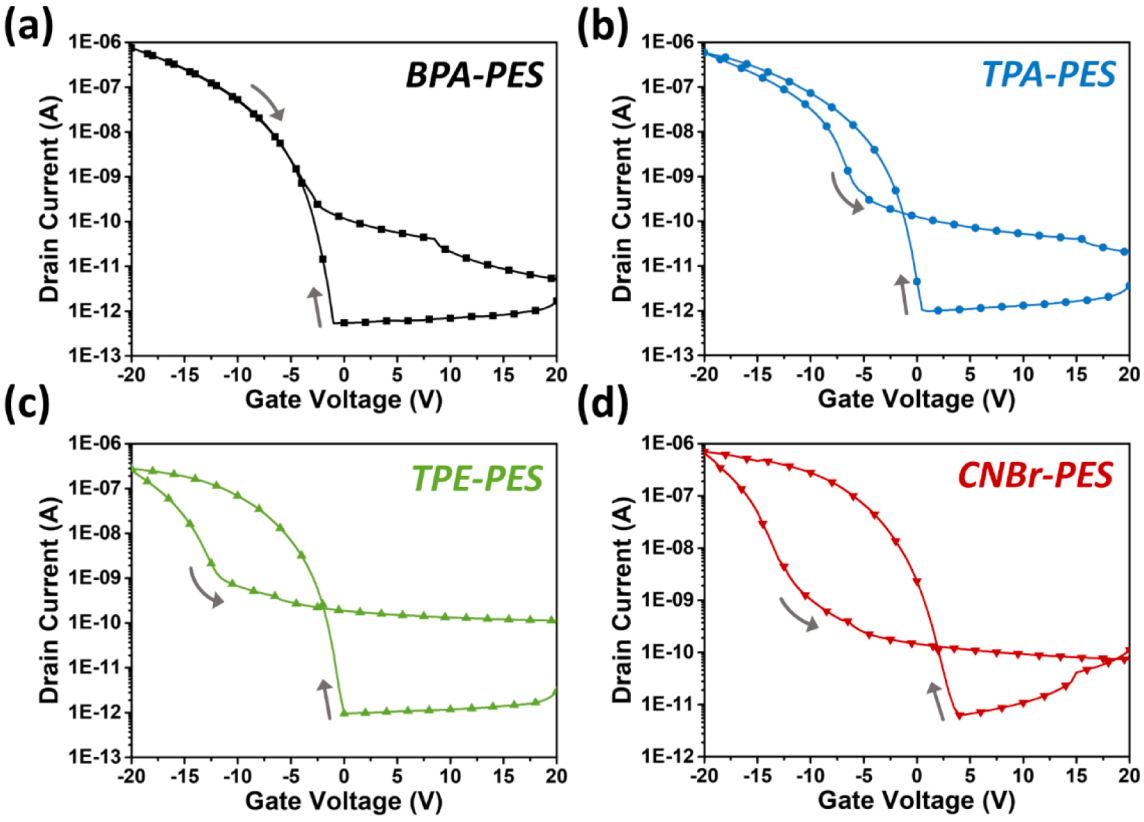

Fig. 6. The hysteresis window of the p-type PESs-based 100 nm SiO_2 OFET memory devices. All currents were measured under a dark environment and fixed drain voltage (V_{DS} = −5 V).

trapping capability [37]. To confirm the electrical memory behaviors based on the relatively low working voltages brought by PESs, a thicker dielectric layer of 300 nm SiO_2 was adopted for memory devices to rule out the leakage current and tunneling effect. Figures S14-S15 depict the typical hole-transporting characteristics of the transfer curve with an on/off current ratio of 10^4 under a fixed drain voltage (V_{DS} = −20 V). The results demonstrate that comparable hole-trapping behavior could be sustained despite the varied gate dielectric thicknesses. However, the 300 nm SiO_2 device possesses the enlargement of memory windows. Based on the constant transferred (stored) charges number ΔN ($\Delta N = C_i \times \Delta V_{th}/e$), ΔV_{th} is the shift of threshold voltage, C_i is the capacitance of the gate dielectric, and e is the elementary charge, which is determined by the charge trapping capability between electret and semiconducting materials, the more oversized memory windows in 300 nm thick SiO_2

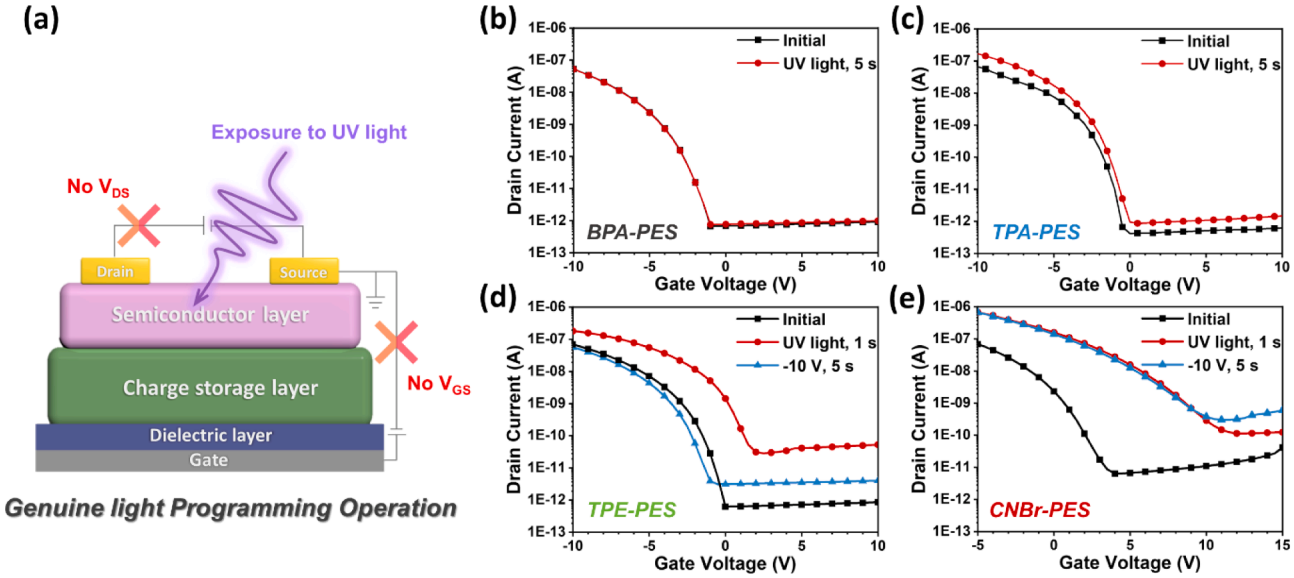

Fig. 7. (a) Diagram of the genuine photo-programming operation that occurs during light exposure without providing the gate and source-drain voltages. (b)-(e) Transfer curves of PESs memory devices based on 100 nm SiO_2 under UV light (365 nm, 5 mW cm^{-2}) photo programming and electric erasing. All currents were measured under a dark environment and fixed drain voltage (V_{DS} = −5 V).

device compared to the 100 nm thick SiO_2 device could ascribe to the smaller capacitance of thicker gate dielectric [38]. Notably, in contrast to the other photoresponsive polymeric electret Poly CD and PTPAs we delivered recently [5,15], the drain voltage could be reduced pronouncedly. The relatively low working voltage could obtain regardless of the oxide thickness, owing to the sturdy pentacene layer built on PESs. The similar trend of electrical characteristics dispels the concern for memory behaviors caused by leakage current or tunneling. Therefore, we utilized a 100 nm SiO_2 layer for the subsequent investigation.

The 365-nm UV light was utilized as the stimulating source to explore the photo-induced characteristics of the PESs-based memory devices without gate and source-drain voltages applied on neutral devices in Fig. 7. The transfer curve of BPA-PES and TPA-PES barely moved; markedly positive shifted transfer curves of TPE-PES and CNBr-PES could be obtained after the illumination.

By prolonging the irradiation time, the TPE-PES and CNBr-PES memory devices could demonstrate more prominent memory windows of 10 V and 50 V, respectively, indicating the photo-produced electrons are trapped into the electret layer successfully, as shown in **Figure S 16**. The dual-layer device comprises pentacene and electret layers, with the former on top and the latter on the bottom. Therefore, under this configuration, both absorbances of organic semiconductor and polymer electrets determine the amount of photoexcited exciton generated. According to absorption spectra in Fig. 3, TPE-PES exhibits the highest absorbance (0.13) at a wavelength of 365 nm, followed by CNBr-PES (0.09) and TPA-PES (0.07), while BPA-PES and pentacene are too low to detect. As mentioned above, when 365 nm light was utilized as the light stimulation, TPE-PES memory devices should exhibit the best optical writing ability. However, CNBr-PES memory devices indicate more extraordinary performance for storing photogenerated electrons under the same illumination source. That is, the absorption intensity at the wavelength of the external light source is merely-one of the elements constructing photo-induce programming behavior.

It needs to note that the pentacene layer could receive substantial energy transfer from the underlying emissive layer, AIE-polymer electrets, with the intense emission in the film state. The behavior of dual-layer excitation, the photoexcitation excitons simultaneously existing in the semiconducting and electret layer, would emerge and facilitate the formation of interlayer-recombined excitons, which subsequently realize the construction of photo-programming. Owing to the emission wavelength of around 575 nm, which is more beneficial to the absorption of pentacene upon UV illumination for generating more interfacial excitons, CNBr-PES memory devices possess the largest memory window among the PESs-based devices. Despite TPE-PES polymer electret having the highest quantum yield, the results demonstrate that the CNBr-PES memory device manifests greater energy transfer efficiency than TPE-PES. Furthermore, the programmed TPE-PES photonic memory device could return to the original neutral state after erasing operations under a lower applying power of just −10 V for 5 s. However, the CNBr-PES-based device could retain most trapped electrons after photo-programming even with reverse-polarity electric stress. In further depth, the following section will go through the differences in storage characteristics between TPE-PES and CNBr-PES.

For the further exploration of the photo-storage phenomenon that converts optical stimulus into electrical signal and preserves at the high current state after light irradiation, the real-time drain currents were recorded at a fixed V_{DS} of −5 V in Fig. 8. The output current contrast ratio is a critical parameter for obtaining a real-time current state in the

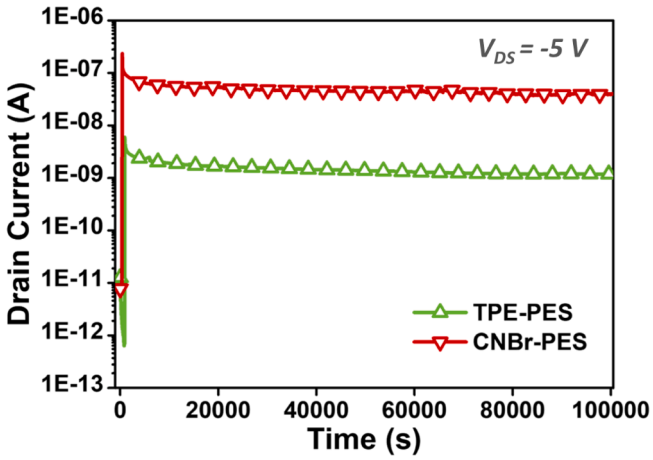

Fig. 9. Long-term stability of TPE-PES and CNBr-PES photonic memory device after programming by 1 s UV light. The retention characteristics of read-out currents were recorded over 100,000 s at V_G = 0 V and 5 V, respectively.

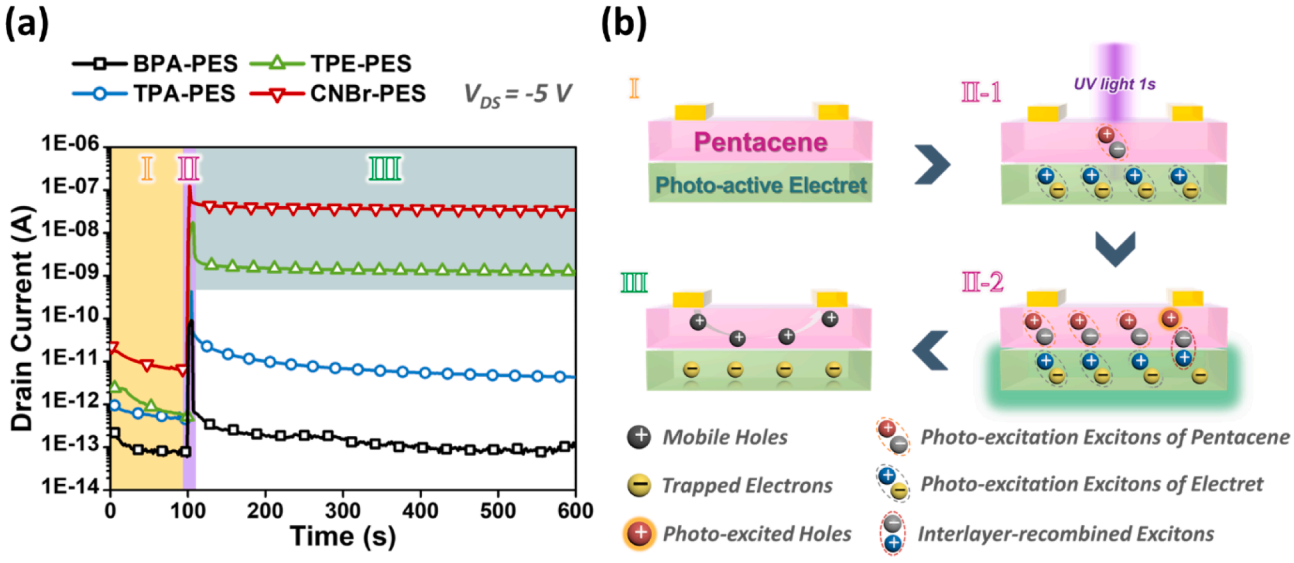

Fig. 8. (a) Transient characteristics of the photonic transistor memory device with PESs-based electret and the corresponding illustration of electret and pentacene layer at "off," "programming," and "on" stages. For optoelectronic stimulative operation, V_{read} = 0 V for BPA-PES, TPA-PES, and TPE-PES memory devices, and V_{read} = 5 V for CNBr-PES memory devices during the irradiation to obtain the real-time read-out currents at V_{DS} = −5 V. (b) Schematic diagrams of the working principle of photo-programming under UV light illumination for the AIE-active PESs electret memory devices.

application of photo-driven memory. Consequently, the memory devices with BPA-PES, TPA-PES, and TPE- PES electrets acquire the off-state stable current (10^{-12} ~ 10^{-13}) without applying gate electric stress (0 V). Nevertheless, 5 V gate bias is necessary to guarantee a decent on/off current ratio to prevent misreading for the CNBr-PES-based device. In Fig. 8**a**, the drain currents remain off-state (<10^{-11} A) for 100 s to ensure stable read-out values and preclude the light influence while settling the device. Afterward, apply UV light (365 nm, 5 mW cm^{-2}) of 1 s to the apparatus for programming operation. During photoexcitation, the light-produced excitons within pentacene can overcome the barrier of binding energy and give charge pairs for accelerating transporting [39]. Consequently, the photo-induced current could generate simultaneously depending on the emission wavelength of PESs that pentacene could absorb [40]. Finally, the devices were steadily read in the dark for 500 s to confirm the memory behaviors. Nevertheless, the current could barely maintain for the BPA-PES-based device, indicating that the electron-withdrawing sulfone group would not perform the electron-trapping characteristic under light illumination. Besides, TPA-PES-based devices could produce less than one order discrepancy between on-current and off-current owing to the inappropriate emission wavelength and low quantum yield resulting in inefficient energy transfer from the electret to the pentacene layer. In contrast, the current from 10^{-12} A increases abruptly up to 10^{-8} A for CNBr-PES and 10^{-9} A for TPE-PES, revealing a "photo-on" characteristic with an on/off current ratio of more than 10^3.

Herein, the possible working mechanism to elucidate the light programmable behavior exhaustively for memory devices using AIE-active PESs polymer as electrets in Fig. 8**b**, which is composed of three successive progressions: Initially, devices maintain a neutral state since the conductive channel could not generate under electrical stress (I). Subsequently, 1 s of UV illumination (365 nm, 5 mW cm^{-2}) for photo-writing was employed. Depending on the absorbance difference of UV light, PES electrets could produce ample photoexcitation excitons, while pentacene generates much fewer photoexcitation excitons (II-1). The simultaneous dual excitation was facilitated through energy transfer from photo-active PESs to pentacene and followed by the recombination of interlayer excitons, allowing the residue electron to trap in the electret layer (II-2). Meanwhile, the high-energy holes from photoexcitation excitons could remain in the semiconductor layer (III). Finally, the trapped electrons could stably store in PESs electret; thence, the devices preserved the high conductive state.

The retention characteristics of devices derived from TPE-PES and CNBr-PES were investigated, as shown in Fig. 9. After photo-programming, all currents could maintain without obvious decay over 100,000 s, demonstrating the nonvolatile nature with outstanding stability, which could be attributed to the soft ether linkage hindering the stacking and avoiding the dissipation by conjugation. According to the extrapolation depicted in **Figure S17**, these PESs-based memory devices could be expected to preserve the switching ratio above 10^3 even over 10^9 s (about 32 years). Furthermore, an upgraded measurement, as shown in **Figure S21**, a stable I_{DS} with negligible variation for the CNBr-PES memory device and slight dissipation for the TPE-PES memory device was obtained for two weeks (more than 1,200,000 s) of measurements, affirming the excellent retention capability of these devices.

As a critical factor in memory device application, the erasing behavior of charged devices could achieve by applying a negative bias. Intriguingly, TPE-PES only required −10 V to recover to the initial state as a Flash-type memory, as shown in Fig. 10. The very low erasing voltage could ascribe to the extended conjugation length, leading to a higher hole affinity and further boosting the neutralization of the trapped electrons presented in the transfer curves. However, the CNBr-PES-based device exhibits non-erasable WORM-type behavior even after applying gate pulse repeatedly 20 times, as illustrated in **Figure S18**, due to the twisted dihedral angle between donor and acceptor groups [15].

Furthermore, the endurance of the Flash-type memory device derived from the TPE-PES electret was demonstrated by write-read-erase-read (WRER) cycles. As illustrated in Fig. 10, the photonic memory device was programmed by UV light for 1 s, and reading on-current, which represents signal "1" for 60 s under V_{DS} = -5 V. Afterwards, a negative bias V_G = −10 V for 5 s was applied to discharge the device and to read off-current as signal "0" for 120 s to complete a cycle. The period of de-trapping for the TPE-PES device has to prolong due to the retarded dissipation of residual charges, which could be related to the high electron affinity of the sulfone group. Despite that, TPE-PES displays superior durability for switching between on and off states over 100 cycles (500 cycles shown in **Figure S22**) without significant degradation in a current ratio of ~10^3.

4. Conclusions

In this study, every building block of triphenylamine-based poly (ether sulfone)s have been elucidated soundly to construct the high-performance photonic transistor memory. The judicious design for a solution-processable charge storage layer of homopolymers could rule out the consideration of dispersion technique, specific morphology, and compromising electrical characteristics. In addition, a facile energy-efficient operation approach for genuine organic photonic memory devices has been proposed via incorporating an AIE-active group (TPE and CNBr), realizing that the photoexcitation electrons could be generated and then remain in the storage layer solely through irradiation without introducing additional electrical stress. Moreover, the synthesized TPA-based PESs possess advantages, such as facile, budgeted, and easily purified polymerization, outstanding thermal stability, and solution

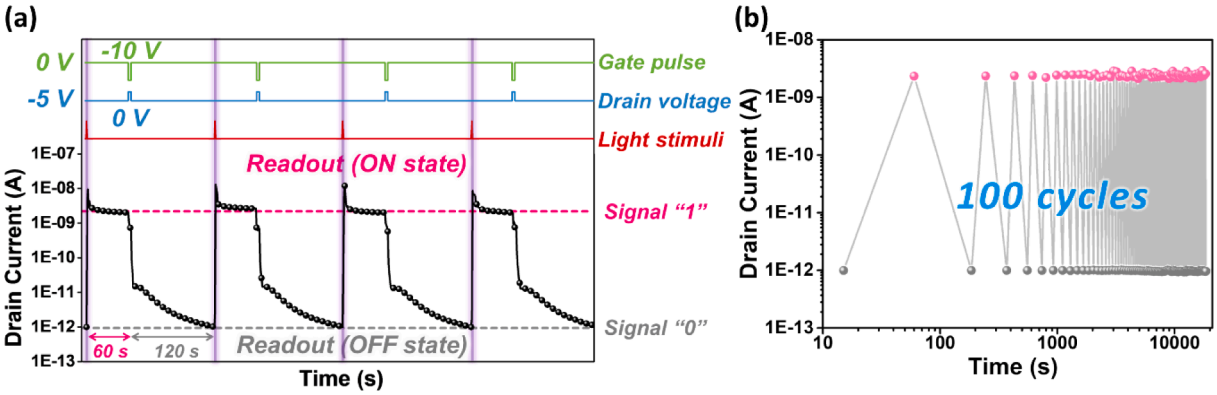

Fig. 10. (a) Reversible current-response behavior under WRER steps for demonstrating the durability of **TPE-PES** device, the applied WRER steps including (i) 1 s UV light (365 nm, 5 mW cm^{-2}) photo-programming (ii) Reading on-state for 60 s (iii) Electrical-erasing (V_G = -10 V for 5 s) (iv) Reading off-state for 120 s. (b) Endurance test of **TPE-PES** for 100 switching cycles.

processability for practical large-area production, and were the first ever employed in OFET memory devices as electret layers. We also demonstrated that a polar and twisted sulfone group could provide a favorable growth environment for pentacene and reduce the contact resistance between semiconducting materials and electrodes, leading to lower working voltage (V_{DS} = −5 V). The results confirm that PES-based photonic memory devices behave with nonvolatile characteristics since PESs constructed with highly distorting ether linkage could restrain the leakage of stored charges, exhibiting remarkable retention of the charged state over 100,000 s. Besides, TPE-PES is a flash-type memory with excellent durability under photo-writing operation for 1 s and electrical erasing operation at −10 V for 5 s. Finally, the prepared PESs with high transparency and manufacturability could further integrate with flexible substrates and become potential candidates in soft and portable optoelectronic devices.

Declaration of Competing Interest

The authors declare that they have no known competing financial interests or personal relationships that could have appeared to influence the work reported in this paper.

Data availability

Data will be made available on request.

Acknowledgments

The authors gratefully acknowledge Prof. Yu-Cheng Chiu and Ms. Mei-Nung Chen at the Department of Chemical Engineering, National Taiwan University of Science and Technology (NTUST), for their assistance in device fabrication, Keithley 4200 measurements and the fruitful discussions. The authors gratefully thank the financial support from the Ministry of Science and Technology in Taiwan (MOST 111-2113-M-002-024 and 111-2221-E-002-028-MY3) and Ms. Huang, Shou-Ling for assistance in NMR experiments in the Instrumentation Center at NTU, supported by the Ministry of Science and Technology, Taiwan.

Appendix A. Supplementary data

Supplementary data to this article can be found online at https://doi.org/10.1016/j.cej.2022.141209.

References

[1] S.T. Han, Y. Zhou, V.A.L. Roy, Towards the development of flexible nonvolatile memories, Adv. Mater. 25 (2013) 5425–5449.
[2] Y. Ni, Y. Wang, W. Xu, Recent process of flexible transistor-structured memory, Small 17 (2021) 1905332.
[3] J.Y. Chen, Y.C. Chiu, Y.T. Li, C.C. Chueh, W.C. Chen, Nonvolatile perovskite-based photomemory with a multilevel memory behavior, Adv. Mater. 29 (2017) 1702217.
[4] S.W. Cheng, T. Han, T.Y. Huang, B.Z. Tang, G.S. Liou, High-performance electrofluorochromic devices based on aromatic polyamides with AIE-active tetraphenylethene and electro-active triphenylamine moieties, Polym. Chem. 9 (2018) 4364–4373.
[5] C.H. Chen, Y. Wang, H. Tatsumi, T. Michinobu, S.W. Chang, Y.C. Chiu, G.S. Liou, Novel photo-induced recovery of OFET memories based on ambipolar polymer electret for photorecorder application, Adv. Funct. Mater. 29 (2019) 1902991.
[6] C.H. Chen, Y. Wang, T. Michinobu, S.W. Chang, Y.C. Chiu, C.Y. Ke, G.S. Liou, Donor-acceptor effect of carbazole-based conjugated polymer electrets on photoresponsive flash organic field-effect transistor memories, ACS Appl. Mater. Interfaces 12 (2020) 6144–6150.
[7] C.Y. Ke, M.N. Chen, Y.C. Chiu, G.S. Liou, Luminescence behavior and acceptor effects of ambipolar polymeric electret on photorecoverable organic field-effect transistor memory, Adv. Electron. Mater. 7 (2021) 2001076.
[8] M.N. Chen, S.W. Chang, S.P. Prakoso, Y.T. Li, K.L. Chen, Y.C. Chiu, Unveiling the photo-induced recovery mystery in conjugated polymer-based transistor memory, ACS Appl. Mater. Interfaces 13 (2021) 44656–44662.
[9] L. Zhang, X. Gao, J. Lv, Y. Zhong, C. Xu, J. Xu, S. Wang, Filter-free selective light monitoring by organic field-effect transistor memories with a tunable blend charge-trapping layer, ACS Appl. Mater. Interfaces 11 (2019) 40366–40371.
[10] M. Wu, S. Shang, Q. Wei, C. Liu, A. Li, X. Gao, S. Wang, J. Yin, Y. Xia, Z. Liu, High visible-light-stimulated plasticity in optoelectronic synaptic transistors for irradiation history-dependent learning, Adv. Electron. Mater. 6 (2020) 1901255.
[11] Z. Zhang, X. Gao, J. Luo, Y. Zhong, J. Xu, S. Wang, UV-enabled multibit organic transistor memory with high controllability and stability, IEEE Electron Device Lett. 43 (2022) 124–127.
[12] Y.C. Chiang, C.C. Hung, Y.C. Lin, Y.C. Chiu, T. Isono, T. Satoh, W.C. Chen, High-performance nonvolatile organic photonic transistor memory devices using conjugated rod-coil materials as a floating gate, Adv. Mater. 32 (2020) 2002638.
[13] B. Mukherjee, M. Mukherjee, Y. Choi, S. Pyo, Control over multifunctionality in optoelectronic device based on organic phototransistor, ACS Appl. Mater. Interfaces 2 (2010) 1614–1620.
[14] Z.Y. Wei, S.P. Prakoso, Y.T. Li, Y.C. Chiu, Tunneling-effect-boosted interfacial charge trapping toward photo-organic transistor memory, Adv. Electron. Mater. 8 (2022) 2101349.
[15] C.Y. Ke, M.H. Chen, Y.T. Li, Y.C. Chiu, G.S. Liou, Novel authentic and ultrafast organic photorecorders enhanced by AIE-active polymer electrets via interlayer charge recombination, Adv. Funct. Mater. 31 (2021) 2101288.
[16] S.D. Wang, T. Miyadera, T. Minari, Y. Aoyagi, K. Tsukagoshi, Correlation between grain size and device parameters in pentacene thin film transistors, Appl. Phys. Lett. 93 (2008), 043311.
[17] R. Hu, A. Qin, B.Z. Tang, AIE polymers: synthesis and applications, Prog. Polym. Sci. 100 (2020), 101176.
[18] R. Hu, Y. Kang, B.Z. Tang, Recent advances in AIE polymers, Polym. J. 48 (2016) 359–370.
[19] H.T. Lin, C.L. Huang, G.S. Liou, Design, synthesis, and electrofluorochromism of new triphenylamine derivatives with AIE-active pendent groups, ACS Appl. Mater. Interfaces 11 (2019) 11684–11690.
[20] S.Y. Chen, Y.W. Chiu, G.S. Liou, Substituent effects of AIE-active α-cyanostilbene-containing triphenylamine derivatives on electrofluorochromic behavior, Nanoscale 11 (2019) 8597–8603.
[21] S.H. Hsiao, H.M. Wang, P.C. Chang, Y.R. Kung, T.M. Lee, Synthesis and electrochromic properties of aromatic polyetherimides based on a triphenylamine-diether amine monomer, J. Polym. Sci. A Polym. Chem. 51 (2013) 2925–2938.
[22] A.X. Ding, H.J. Hao, Y.G. Gao, Y.D. Shi, Q. Tang, Z.L. Lu, D-A-D type chromophores with aggregation-induced emission and two-photon absorption: synthesis, optical characteristics and cell imaging, J. Mater. Chem. C 4 (2016) 5379–5389.
[23] Y. Liu, X. Chen, Y. Lv, S. Chen, J.W.Y. Lam, F. Mahtab, H.S. Kwok, X. Tao, B. Z. Tang, Systemic studies of tetraphenylethene-triphenylamine oligomers and a polymer: achieving both efficient solid-state emissions and hole-transporting capability, Chem. Eur. J. 18 (2012) 9929–9938.
[24] B.K. An, S.K. Kwon, S.D. Jung, S.Y. Park, Enhanced emission and its switching in fluorescent organic nanoparticles, J. Am. Chem. Soc. 124 (2002) 14410–14415.
[25] Y. Wang, X. Huang, T. Li, L. Li, X. Guo, P. Jiang, Polymer-based gate dielectrics for organic field-effect transistors, Chem. Mater. 31 (2019) 2212–2240.
[26] H.S. Lee, D.H. Kim, J.H. Cho, M. Hwang, Y. Jang, K. Cho, Effect of the phase states of self-assembled monolayers on pentacene growth and thin-film transistor characteristics, J. Am. Chem. Soc. 130 (2008) 10556–10564.
[27] S.E. Fritz, T.W. Kelley, C.D. Frisbie, Effect of dielectric roughness on performance of pentacene TFTs and restoration of performance with a polymeric smoothing layer, J. Phys. Chem. B 109 (2005) 10574–10577.
[28] R. Ruiz, D. Choudhary, B. Nickel, T. Toccoli, K.C. Chang, A.C. Mayer, P. Clancy, J. M. Blakely, R.L. Headrick, S. Iannotta, G.G. Malliaras, Pentacene thin film growth, Chem. Mater. 16 (2004) 4497–4508.
[29] S. Steudel, S. De Vusser, S. De Jonge, D. Janssen, S. Verlaak, J. Genoe, P. Heremans, Influence of the dielectric roughness on the performance of pentacene transistors, Appl. Phys. Lett. 85 (2004) 4400–4402.
[30] Y. Baek, S. Lim, E.J. Yoo, L.H. Kim, H. Kim, S.W. Lee, S.H. Kim, C.E. Park, Fluorinated polyimide gate dielectrics for the advancing the electrical stability of organic field-effect transistors, ACS Appl. Mater. Interfaces 6 (2014) 15209–15216.
[31] M. Jang, M. Lee, H. Shin, J. Ahn, M. Pei, J.H. Youk, H. Yang, Balancing surface hydrophobicity and polarizability of fluorinated dielectrics for organic field-effect transistors with excellent gate-bias stability and mobility, Adv. Mater. Interfaces 3 (2016) 1600284.
[32] H. Zhao, L. Yang, X. Chen, M. Sheng, G. Cao, L. Cai, S. Meng, C.Y. Tang, Degradation of polyamide nanofiltration membranes by bromine: changes of physiochemical properties and filtration performance, Environ. Sci. Technol. 55 (2021) 6329–6339.
[33] I. Akiba, A. Takechi, M. Sakou, M. Handa, Y. Shinohara, Y. Amemiya, N. Yagi, K. Sakurai, Anomalous small-angle X-ray scattering study of structure of polymer micelles having bromines in hydrophobic core, Macromolecules 45 (2012) 6150–6157.
[34] L.J. Anderson, R.B. Moore, Sulfonation of blocky brominated PEEK to prepare hydrophilic-hydrophobic blocky copolymers for efficient proton conduction, Solid State Ion. 336 (2019) 47–56.
[35] D. Ji, X. Xu, L. Jiang, S. Amirjalayer, L. Jiang, Y. Zhen, Y. Zou, Y. Yao, H. Dong, J. Yu, H. Fuchs, W. Hu, Surface polarity and self-structured nanogrooves collaboratively oriented molecular packing for high crystallinity toward efficient charge transport, J. Am. Chem. Soc. 139 (2017) 2734–2740.
[36] S.D. Wang, T. Minari, T. Miyadera, K. Tsukagoshia, Y. Aoyagi, Contact-metal dependent current injection in pentacene thin-film transistors, Appl. Phys. Lett. 91 (2007), 203508.
[37] J.C. Hsu, W.Y. Lee, H.C. Wu, K. Sugiyama, A. Hirao, W.C. Chen, Nonvolatile memory based on pentacene organic field-effect transistors with polystyrene para-substituted oligofluorene pendent moieties as polymer electrets, J. Mater. Chem. 22 (2012) 5820–5827.

[38] K.J. Baeg, Y.Y. Noh, J. Ghim, S.J. Kang, H. Lee, D.Y. Kim, Organic nonvolatile memory based on pentacene field-effect transistors using a polymeric gate electret, Adv. Mater. 18 (2006) 3179–3183.
[39] K.J. Baeg, M. Binda, D. Natali, M. Caironi, Y.Y. Noh, Organic light detectors: photodiodes and phototransistors, Adv. Mater. 25 (2013) 4267–4295.
[40] S. Dutta, K.S. Narayan, Gate-voltage control of optically-induced charges and memory effects in polymer field-effect transistors, Adv. Mater. 16 (2004) 2151–2155.